© 2019. Published by The Company of Biologists Ltd | Development (2019) 146, dev181487. doi:10.1242/dev.181487

RESEARCH ARTICLE

Dynamics of Spaetzle morphogen shuttling in the *Drosophila* embryo shapes gastrulation patterning

Neta Rahimi*, Inna Averbukh*, Shari Carmon, Eyal D. Schejter, Naama Barkai‡ and Ben-Zion Shilo‡

ABSTRACT

Establishment of morphogen gradients in the early *Drosophila* embryo is challenged by a diffusible extracellular milieu, and by rapid nuclear divisions that occur at the same time. To understand how a sharp gradient is formed within this dynamic environment, we followed the generation of graded nuclear Dorsal protein, the hallmark of pattern formation along the dorso-ventral axis, in live embryos. The dynamics indicate that a sharp extracellular gradient is formed through diffusion-based shuttling of the Spaetzle (Spz) morphogen that progresses through several nuclear divisions. Perturbed shuttling in *wntD* mutant embryos results in a flat activation peak and aberrant gastrulation. Re-entry of Dorsal into the nuclei at the final division cycle plays an instructive role, as the residence time of Dorsal in each nucleus is translated to the amount of zygotic transcript that will be produced, thereby guiding graded accumulation of specific zygotic transcripts that drive patterned gastrulation. We conclude that diffusion-based ligand shuttling, coupled with dynamic readout, establishes a refined pattern within the diffusible environment of early embryos.

KEY WORDS: *Drosophila* embryo, Morphogen gradient, Patterning dynamics, Toll signaling, Shuttling

INTRODUCTION

The crude onset and subsequent refinement of spatial information shape the future body pattern of embryos. Morphogens, key instructive elements in this context, are secreted signaling molecules that induce cells to adopt different fates depending on the morphogen concentration they experience. Establishing a morphogen gradient over a field of naïve cells patterns the cell layer into distinct domains of gene expression (Green and Sharpe, 2015; Wolpert, 1971). A common strategy for generating a morphogen gradient is to produce the morphogen in a restricted group of cells, giving rise to its graded distribution in the surrounding cells (Lecuit et al., 1996; Nellen et al., 1996). In this scenario, the morphogen-producing cells are typically distinct from the responding cells.

An alternative strategy of morphogen distribution is applicable to situations in which the morphogen is broadly expressed, and the gradient is generated within the field of expressing cells. This scenario is applicable to early embryos, in which broad transcriptional domains have been established, but these domains are not sufficiently restricted to provide for a local morphogen source. In such situations, restricting morphogen signaling to a narrow domain becomes a challenge, as diffusion tends to spread, rather than restrict, ligand distribution.

Studies in several systems identified the 'shuttling' mechanism as a robust solution to this challenge (Shilo et al., 2013). Here, a morphogen gradient is established not merely by its diffusion away from the production source, but through an effective translocation of the morphogen into the center of the field. This translocation is purely diffusion driven, and is mediated by a distally produced inhibitor. The resulting gradient is sharp and robust, displaying limited sensitivity to gene dosages or reaction rate constants. Shuttling provides robustness by concentrating the morphogen into a restricted domain, which allows excess levels to be stored in regions of maximal signaling, without modifying the resulting cell fates. Morphogen gradients established by the shuttling mechanism include the bone morphogenetic protein (BMP) gradient in the early embryos of *Drosophila*, other insects and sea urchins (Eldar et al., 2002; Lapraz et al., 2009; Shimmi et al., 2005; van der Zee et al., 2006; Wotton et al., 2017). Shuttling is also used for forming the BMP gradient in *Cnidaria* (Genikhovich et al., 2015) and in the *Xenopus* embryo, where it has acquired additional features that allow for scaling of the gradient with embryo size (Ben-Zvi et al., 2014, 2008).

Compelling evidence for shuttling was provided by comparing mutant phenotypes with the predictions made by computational models (Ben-Zvi et al., 2008; Eldar et al., 2002; Haskel-Ittah et al., 2012). It was also demonstrated that ligand produced ectopically in one part of the embryo can be translocated to its normal activity zone, defined by the expression domain of the shuttling molecule (Reversade and De Robertis, 2005; Wang and Ferguson, 2005). Experimentally, these data were obtained through the analysis of fixed embryos. Yet, the essence of the gradient-forming mechanisms resides in their dynamics. What is the time frame during which the gradient is established? How fast is gradient formation relative to its readout, i.e. does the resulting gene expression take place after the gradient was formed and refined by shuttling or does gene expression respond dynamically to the continuous sharpening of the gradient? Furthermore, considering the dynamic environment of the early embryo – where the nuclei undergo multiple division cycles during which their environment is perturbed – is the gradient stably formed, or is it subject to subsequent cycles of refinement? Insight into these questions requires monitoring the dynamic distribution of the morphogen within living single embryos.

The ability to observe the dynamics of morphogen gradient formation is challenging because the ligands typically function at low levels. Furthermore, the morphogen may be present not only in its active form, but also in a non-processed, inactive form, or bound to an inhibitor. Finally, the morphogen is present in both extra- and intracellular locations. Most studies therefore follow the patterning processes by quantifying the intracellular outcome of morphogen signaling as a proxy for active morphogen distribution, using

Department of Molecular Genetics, Weizmann Institute of Science, Rehovot 7610001, Israel.
*These authors contributed equally to this work

‡Authors for correspondence (naama.barkai@weizmann.ac.il; benny.shilo@weizmann.ac.il)

E.D.S., 0000-0001-6093-5973; N.B., 0000-0002-2444-6061; B.-Z.S., 0000-0003-4903-8889

Received 13 June 2019; Accepted 7 October 2019

Development (2019) 146, dev181487. doi:10.1242/dev.181487

antibodies against the activated (e.g. phosphorylated) states of signaling pathways triggered by morphogens (Dorfman and Shilo, 2001; Gabay et al., 1997; Tanimoto et al., 2000). Such approaches, however, cannot be used to follow live embryos, as they rely on immunostaining of fixed samples. An alternative is to follow the transcriptional outcomes of morphogen signaling, but this analysis is already quite removed from the original morphogen gradient itself, and is compounded by additional regulatory inputs controlling the expression of the target genes.

Patterning the dorso-ventral (D-V) axis of the *Drosophila* embryo provides a powerful system in which to analyze the dynamics of morphogen gradient formation (Lynch and Roth, 2011). The early *Drosophila* embryo is a syncytium, i.e. a collection of nuclei that occupy a common cytoplasm enclosed by the embryonic plasma membrane. Within this syncytium, the nuclei undergo 13 rapid and synchronous divisions without any change in embryo size or shape. During the final four division cycles, the nuclei form a monolayer just beneath the plasma membrane (Foe and Alberts, 1983; Schejter and Wieschaus, 1993). The signaling protein Spaetzle (Spz) is secreted from the syncytium into the surrounding peri-vitelline fluid, positioned between the plasma and vitelline membranes, and a gradient of active Spz forms within it, along the radial D-V axis. The processed Spz morphogen binds the transmembrane Toll receptor positioned on the plasma membrane (DeLotto and DeLotto, 1998; Morisato and Anderson, 1994; Schneider et al., 1994; Weber et al., 2003), and the resulting signaling pathway triggers translocation of the transcription factor Dorsal into the syncytial nuclei. The processed form of the Spz ligand therefore functions as the morphogen at this stage.

We previously showed that graded active Spz distribution is established by a shuttling mechanism. In this case, shuttling is implemented in a self-organized manner through interplay between the active ligand and its pro-domain, which can accommodate diverse structures. Cleavage of the covalent link between the Spz pro-domain and the ligand retains the association between the two moieties but allows binding to Toll. Upon binding, the pro-domain is released. Occasionally the active ligand may also dissociate. Re-association between the ligand and the pro-domain generates an inactive complex that translocates the active ligand to the ventral midline (Fig. 1A,B) (Haskel-Ittah et al., 2012; Shilo et al., 2013). Shuttling results in a sharp ventral gradient of active Spz (Fig. 1C), and provides robustness to a variety of perturbations in the level of pathway components.

To visualize the dynamics of gradient formation, we considered the nuclear localization of Dorsal, a direct output of Spz signaling. Entry of Dorsal into the nuclei can be followed in single live embryos carrying a Dorsal-GFP fused protein (DeLotto et al., 2007). We use light-sheet fluorescence microscopy (LSFM) for live imaging of Dorsal-GFP nuclear localization during the final nuclear division cycles of the syncytial *Drosophila* embryo. The resulting dynamics show the two signatures of ligand shuttling within the broad ventral domain: a transient increase in signaling in the lateral regions, which is then reduced in order to preferentially increase signaling at the ventral midline, and the resolution of two lateral peaks to a single central (midline) peak.

We find that ligand shuttling is an ongoing process, which repeats itself following each nuclear division. Further, nuclear re-entry of Dorsal at the beginning of nuclear cycle 14 refines the spatial pattern of gradient readout, as closely positioned nuclei begin to express key zygotic target genes at slightly different times. This converts the morphogen gradient information to a graded cytoplasmic distribution of zygotic transcripts, which subsequently impinge on the pattern of gastrulation. The secreted protein WntD, an inhibitor of Toll signaling, buffers the D-V patterning gradient against fluctuations through an integral negative feedback (Rahimi et al., 2016). We now find that in *wntD* mutant embryos, the Dorsal peak becomes flattened, and leads to an abnormal increase in the number of cells simultaneously undergoing the initial step of gastrulation, highlighting the significance of properly shaped gradient formation. Thus, diffusion-based ligand shuttling, coupled with a dynamic readout, establishes a refined spatial pattern within the environment of early embryos.

RESULTS

Extrapolating the temporal evolution of the Spz gradient during nuclear cycles 12-14

The shuttling mechanism makes a number of counter-intuitive predictions regarding the dynamics of pattern formation. In particular, it predicts that signaling at positions that are at an intermediate distance from the center of the field will initially increase, as the ubiquitously produced ligand begins to accumulate, but will subsequently be reduced, because ligand is continuously being shuttled to the center of the field. This non-monotonic behavior is a defining property of the shuttling mechanism that concentrates ligand, but is absent from other diffusion-based mechanisms that establish a graded pattern. In a certain parameter range, shuttling also predicts transient formation of a double-peak pattern, as a consequence of the gradual ventral translocation of ligand from the two lateral edges. This property is also absent from naïve gradient-forming mechanisms that display temporally monotonic behavior throughout the tissue. Uncovering such features is possible only by monitoring the dynamics of gradient formation in live embryos.

Using LSFM, we followed individual embryos carrying a Dorsal-GFP fusion protein expressed under the endogenous *dl* promoter (Fig. 1D, Movie 1). Consistent with previous reports (DeLotto et al., 2007; Kanodia et al., 2009), we observed a D-V gradient of nuclear Dorsal-GFP already at nuclear cycle (NC) 12. This gradient was further refined and elaborated during the next two cycles. To enable quantitative analysis of Dorsal-GFP nuclear dynamics, we used an area-preserving transformation to project the 3D images onto a 2D sheet. We restricted our analysis to a region surrounding the antero-posterior (A-P) midline, where distortion due to 2D projection is negligible (Fig. 1E, Movies 2 and 3) (Heemskerk and Streichan, 2015). Next, we automatically segmented the nuclei and averaged the nuclear Dorsal-GFP signal over nuclei occupying a similar D-V axis position (Materials and Methods; Fig. S1).

Our measurements defined the quantitative, spatio-temporal dynamics of Dorsal-GFP at a 1-2 min time resolution (Fig. 1E,F; Materials and Methods). These dynamics are likely dictated by the extracellular active Spz gradient. However, inferring the profile of this extracellular gradient from Dorsal-GFP dynamics is confounded by the fact that Dorsal nuclear accumulation is established anew at every nuclear cycle, because Dorsal exits the nucleus at mitosis upon nuclear envelope breakdown. We therefore needed a framework to suitably infer properties of the extracellular active Spz gradient, and distinguish between models of gradient formation.

Toll signaling, at each given position along the D-V gradient, defines the rate by which Dorsal is translocated to the nucleus. Thus, at the beginning of each division cycle, following re-establishment of the nuclear envelope and before significant Dorsal nuclear accumulation is observed, nuclear Dorsal levels increase at a rate that is proportional to the level of nearby Toll signaling. Conversely, at later time points, nuclear Dorsal levels approach a steady state that is proportional to the extracellular Toll signaling itself. We therefore

Development (2019) 146, dev181487. doi:10.1242/dev.181487

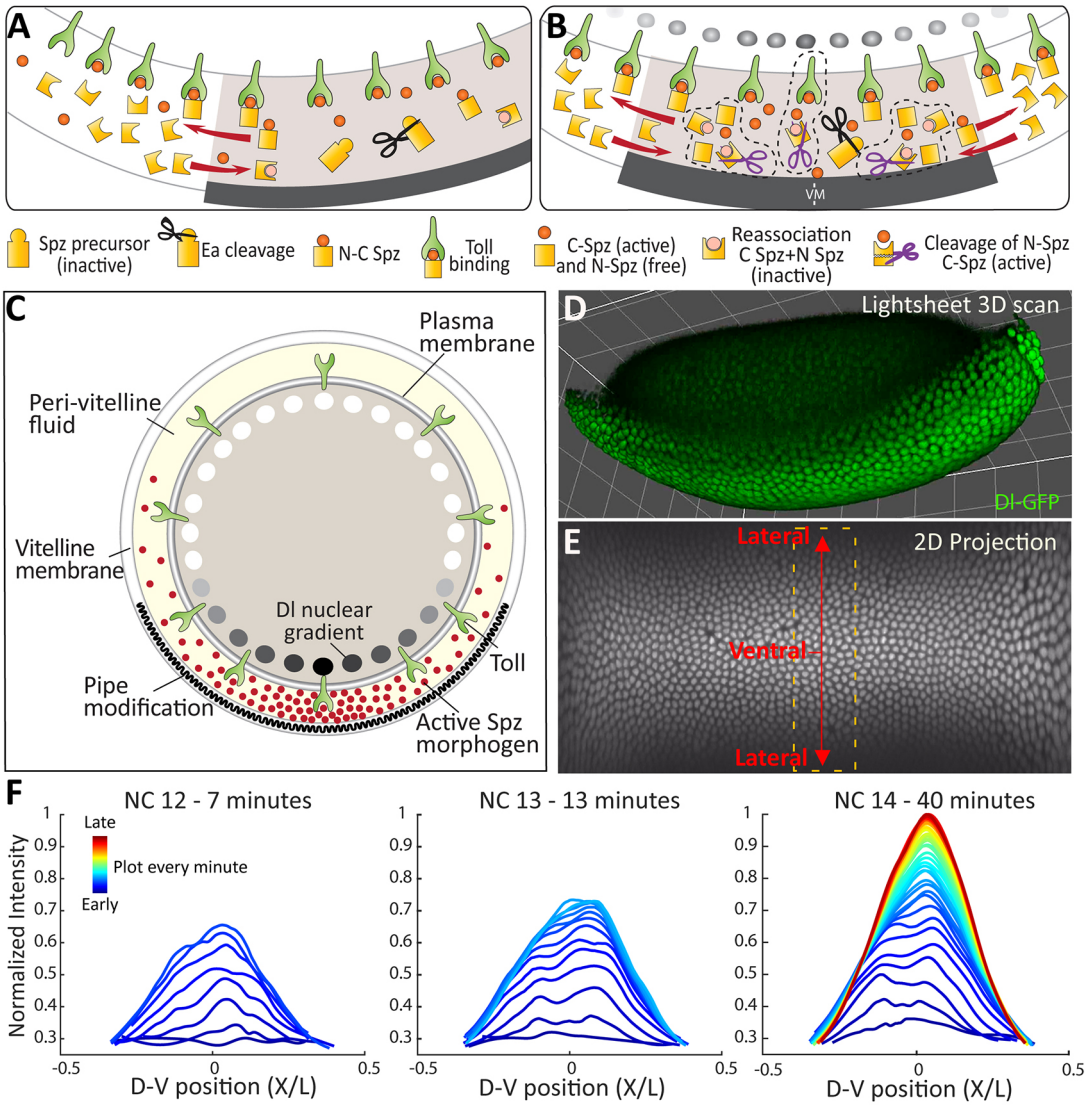

Fig. 1. Dynamics of Dorsal nuclear localization. (A,B) Biochemical versatility of the Spz ligand allows it to function in several distinct forms. It first appears as an inactive ligand. Following cleavage by Easter (Ea) that is restricted to the ventral domain (dark gray bar), the two parts remain non-covalently associated, and can bind the Toll receptor. This leads to dissociation of the Spz pro-domain (N-Spz). The active ligand (C-Spz) and the pro-domain can re-associate, to form an inactive complex. Proposed cleavage of the pro-domain within this complex, will release the active ligand (dashed lines). These molecular features provide the basis for self-organized shuttling of active Spz (Haskel-Ittah et al., 2012). VM, ventral midline. (C) Schematic cross-section of an early embryo after completion of shuttling: Spz is assumed to be distributed in a sharp gradient along the D-V axis within the peri-vitelline space. Spz binding to the Toll receptor triggers a signaling cascade, culminating in a gradient of nuclear Dorsal with a sharp ventral peak. (D) A frame from a light-sheet time-lapse movie following the dynamics of endogenously expressed Dorsal-GFP in the entire embryo. The gradient can be visualized already at NC 12, it is lost during nuclear divisions and is re-generated at the onset of each nuclear cycle. (E) Each frame of the 3D light-sheet scan was projected to a 2D map using the ImSAnE tool (Heemskerk and Streichan, 2015). Here, the 2D projection of the frame from D is shown. The quantification of Dorsal-GFP intensity in the nuclei along the D-V axis at 1 min intervals was carried out on nuclei inside the dashed frame. This region, which is close to the middle of the A-P axis, is not distorted by the 2D projection (see Materials and Methods). (F) Dorsal-GFP intensity, plotted as a function of relative location along the D-V axis [the relative location axis X/L is defined as the location divided by the embryo circumference (see Materials and Methods)]. A curve is shown for each time point for NC 12, 13 and 14 for the same wild-type embryo. Each Dorsal-GFP intensity curve was smoothened and normalized by the maximal value attained during NC 14 (see Materials and Methods). Time points are 1 min apart, going from earliest time points in blue to the latest in red. The duration of each NC in minutes is indicated above the plot.

plotted the dynamics of both parameters, nuclear Dorsal levels and its temporal derivative, during the course of NC 14. Notably, we observed that these qualitative dynamics differ, depending on the spatial position of nuclei along the D-V axis. In the ventral-most regions they increased monotonically. In contrast, in lateral domains nuclear Dorsal displayed an overshoot, initially increasing but then starting to decrease (Fig. 2A-D, Fig. S2). Clearly, such a decrease in nuclear Dorsal is only possible if Toll signaling at this position decreases as well. Therefore, the data suggests that the external Spz gradient continues to evolve through the early part of NC 14, showing a distinct position-dependent, non-monotonic temporal signature.

To more rigorously infer dynamic properties of the external gradient from the measured pattern of nuclear Dorsal, we used computer simulations, modeling Dorsal nuclear entry while assuming different temporal patterns of Toll signaling (Fig. 2E-L). Specifically, we searched for a qualitative signature that distinguishes between three scenarios: (1) Toll signaling that is monotonically

Development (2019) 146, dev181487. doi:10.1242/dev.181487

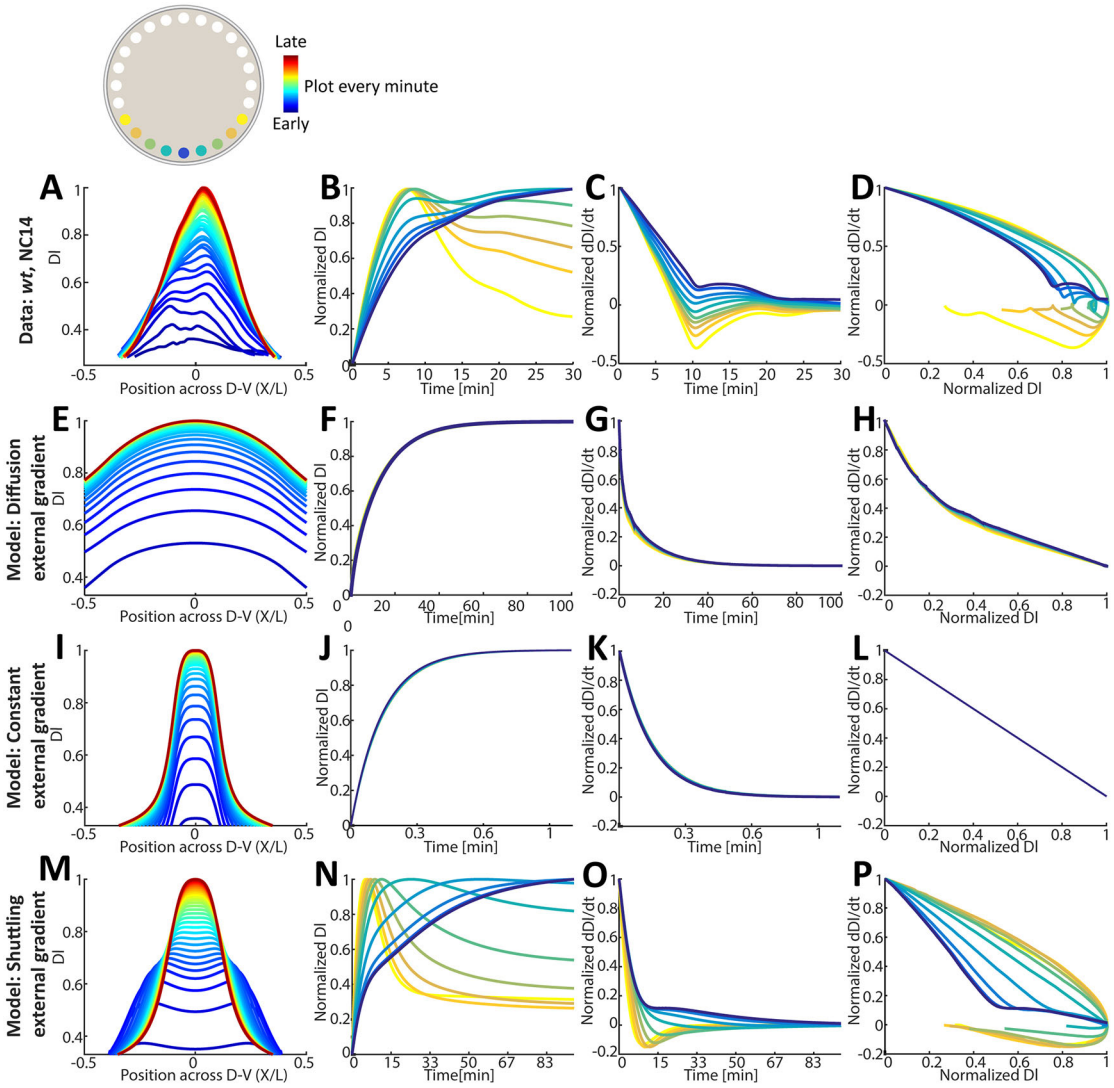

Fig. 2. Measured nuclear Dorsal dynamics during NC 14 indicates ongoing shuttling. (A-D) Measured nuclear Dorsal temporal dynamics for a wild-type embryo; time points are color coded and are 1 min apart. (E-P) Simulations of nuclear Dorsal temporal dynamics (see supplementary Materials and Methods, Table S1). (E-H) Diffusion model: nuclear Dorsal localization induced by Spz binding the Toll receptor, with Spz diffusing out of a wide source while being degraded. (I-L) Constant external gradient model: nuclear Dorsal localization induced by Spz binding the Toll receptor, with a Spz gradient that is constant in time. (M-P) Full model: nuclear Dorsal localization induced by Spz binding the Toll receptor, with shuttling of Spz. (A,E,I,M) Nuclear Dorsal levels in arbitrary units, plotted as a function of the relative location along the D-V axis. A curve is shown for each time point, time points are color coded. (B,F,J,N) Nuclear Dorsal levels at specific locations along the D-V axis, as a function of time. Nuclear localizations along the D-V axis are color coded. Each location's curve was normalized to its own maximal value. (C,G,K,O) Nuclear Dorsal temporal derivative at specific locations along the D-V axis, as a function of time. Each location's curve was normalized to its own maximal value. (D,H,L,P) Nuclear Dorsal temporal derivative at specific locations along the D-V axis, as a function of nuclear Dorsal. Each location's curve was normalized to its own maximal value. Color codes for the temporal dynamics and for the location of nuclei along the D-V axis are shown above.

increasing in time, as expected in naïve gradient-forming models; (2) temporally constant Toll signaling; and (3) Toll signaling formed by a shuttling mechanism, giving rise to non-monotonic behavior in lateral regions. Our simulations showed that these scenarios are best distinguished by comparing the derivative of changes in nuclear Dorsal [d(Dl)/dt] with the levels of nuclear Dorsal. In the first two cases – constant or monotonically increasing Toll activity – the relationship between these two parameters was invariably linear or concave (Fig. 2E-L). In contrast, in a regime of shuttling-based dynamics, a convex relation was obtained, with a pronounced negative temporal derivative at the lateral regions (Fig. 2M-P).

The measured data are not consistent with dynamics that are defined by a monotonically increasing or a constant Toll signaling. Rather, it shows a clear signature of shuttling-like dynamics. Our simulations, which include the full shuttling model that establishes the active Spz gradient combined with Dorsal nuclear transport (see supplementary Materials and Methods), confirmed that this model is fully capable of recapitulating the experimentally observed dynamics, including the overshoot at the lateral regions.

An additional notable property of Dorsal nuclear entry dynamics was the initial formation, at every nuclear cycle, of two ventro-lateral signaling peaks, that eventually converge to a single ventral peak (Figs 1F and 2A, Fig. S2). Thus, by 10-15 min into NC 14, when the robust expression of zygotic Dorsal-target genes is induced, the initial two-peak gradient had refined to a single sharp peak. The initial two-peak pattern provides another unique signature of the shuttling dynamics. This is expected when parameters are such that the mean

Development (2019) 146, dev181487. doi:10.1242/dev.181487

distance traveled by the shuttling complex before it is cleaved is much smaller than the distance to the ventral-most site. In this case, ligand will initially accumulate at lateral regions, followed by gradual ventral translocation (see supplementary Materials and Methods).

Although a sharp peak was observed at the end of NC 12 and NC 13, at the onset of the following cycle the pattern of nuclear Dorsal exhibited a double peak that converges over time to a sharp peak. The reappearance of the double peak at every nuclear cycle may reflect a process of extracellular ligand mixing in the peri-vitelline fluid, possibly caused by reorganization of the cortical actin-based cytoskeleton and deformation of the plasma membrane associated with the nuclear divisions (di Pietro and Bellaïche, 2018; Zhang et al., 2018).

Following Toll activation, the nuclear entry of Dorsal is facilitated by degradation of the Cactus (Cact) protein, which normally retains Dl in the cytoplasm (Belvin and Anderson, 1996). *cact* mutant embryos exhibit a general elevation in nuclear Dorsal levels. However, on top of this elevated background, peak ventral signaling is still observed due to Toll-mediated phosphorylation of Dorsal, which promotes its nuclear entry (Rahimi et al., 2016).

Previous work has suggested that the ventrally biased degradation of Cact may generate a cytoplasmic flux of Dorsal towards the ventral midline (Carrell et al., 2017). To determine whether the shuttling hallmarks we observed stem from extracellular Spz shuttling or intracellular Dorsal shuttling by Cact, we examined the dynamic distribution of nuclear Dorsal in *cact* knockdown embryos (Fig. 3A,B). If Cact-mediated intracellular shuttling is a significant driving force of the dynamics we observed, we anticipate elimination of shuttling signatures in this mutant background. This, however, was not the case: a double peak that converges to a single peak was also observed in *cact* knockdown embryos, and in fact appears to be even more prominent than that detected in wild-type embryos (Fig. 3C,D, Fig. S3). Note that, due to the expected global elevation in Toll signaling, it was not possible to reliably follow the feature of overshoot in lateral nuclei.

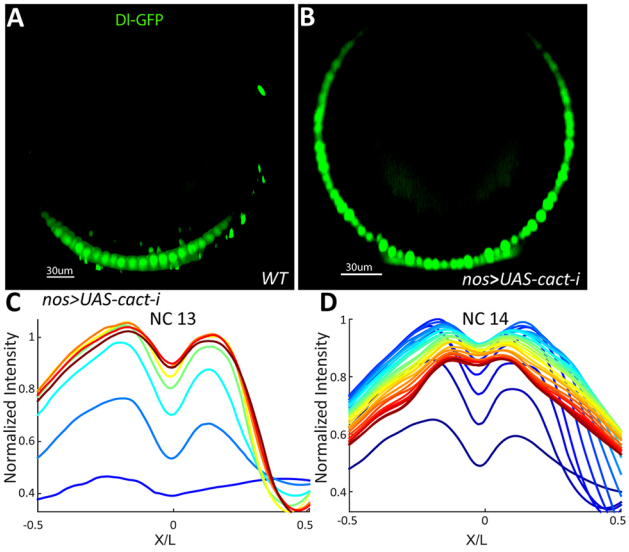

Fig. 3. Shuttling hallmarks are retained in *cact* knockdown embryos. (A) Dorsal-GFP nuclear localization in a wild-type (WT) embryo, displaying a gradient centered at the ventral midline. (B) Knockdown of *cact* by maternal expression of an RNAi construct leads to expansion of Dorsal nuclear localization towards the lateral and dorsal domains. (C,D) Dynamics of Dorsal nuclear localization in a single *cact* knockdown embryo at NC 13 and 14 shows a prominent double peak, which converges towards the ventral midline only during NC 14. Owing to the general increase in Toll pathway signaling, it was not possible to detect its early lateral overshoot. We conclude that the shuttling features observed in wild-type embryos are not generated by shuttling within the cytoplasm, but are driven by extracellular ligand movement.

In conclusion, the dynamic behavior of Dorsal-GFP supports a continuous process of extracellular Spz shuttling, displaying two of its defining signatures: non-monotonic dynamics of nuclear Dorsal entry in lateral regions, and the transient formation of a double-peaked gradient.

Altered shuttling dynamics in *wntD* mutants affects gastrulation

Dorsal nuclear localization dynamics can be used for refined analysis of mutant phenotypes. We applied this approach to study WntD, an inhibitor of Toll signaling which provides a negative feedback that buffers the D-V patterning gradient against fluctuations (Rahimi et al., 2016). *wntD*, itself a target of the Toll pathway, is transcribed locally at the posterior terminus of the embryo, and the secreted protein diffuses within the peri-vitelline fluid to attenuate Toll signaling (Fig. 4A) (Helman et al., 2012; Rahimi et al., 2016).

Upon binding to the Frizzled 4 (Fz4) receptor, WntD is anchored to the membrane. Genetic epistasis experiments are consistent with WntD association with the extracellular domain of Toll, compromising Toll's capacity to bind Spz (Rahimi et al., 2016) (Fig. 4B). However, the consequences of this inhibition on gradient formation remained unclear. One possibility is that WntD uniformly decreases signaling in all regions. Alternatively, with the shuttling mechanism in mind, our simulations suggested that the binding of WntD to the extracellular domain of Toll promotes ligand shuttling. More specifically, within the model, binding of WntD to the Toll receptor decreases the number of available receptors, thus decreasing signaling preferentially in lateral regions and sharpening the gradient. Reducing the number of free receptors further compromises the ability of Spz to bind Toll, thereby increasing the probability that it will bind the free shuttling molecule, leading to more effective shuttling. Uniform distribution of moderate WntD levels would therefore result in redistribution of the ligand to more ventral regions, impacting not only the strength of Toll signaling, but also sharpness of its gradient (see Fig. 4C,F for simulation results, and supplementary Materials and Methods for model details).

Using live imaging in a *wntD* mutant background, we directly tested the impact of WntD on shuttling. The initial signature of a double peak was more prominent and persistent, consistent with higher signaling levels in the absence of WntD. Identification of shuttling in this background indicates that the core mechanisms of shuttling are still operating in the absence of WntD. However, in contrast to wild-type embryos, in which gradual sharpening of the gradient takes place, in a *wntD*-mutant background the final gradient was relatively wide and displayed a flattened, single peak (Fig. 4C-J, Fig. S4), consistent with the predicted role of WntD in promoting the ventral translocation of the Spz ligand (Fig. 4K,L).

To follow the morphological consequences of a wider peak of nuclear Dorsal distribution, we monitored *wntD* mutant embryos for an extended period of NC 14, observing the processes of gastrulation and ventral furrow formation. We defined the edges of the furrowing domain by marking the two lateral-most nuclei that alter their angle with respect to the embryo circumference upon gastrulation. Working backwards to an earlier phase of NC 14, when the nuclei are still in a monolayer, we can accurately count the number of nuclei between these edges. In contrast to gastrulating wild-type embryos, in which the initial invagination was observed

Development (2019) 146, dev181487. doi:10.1242/dev.181487

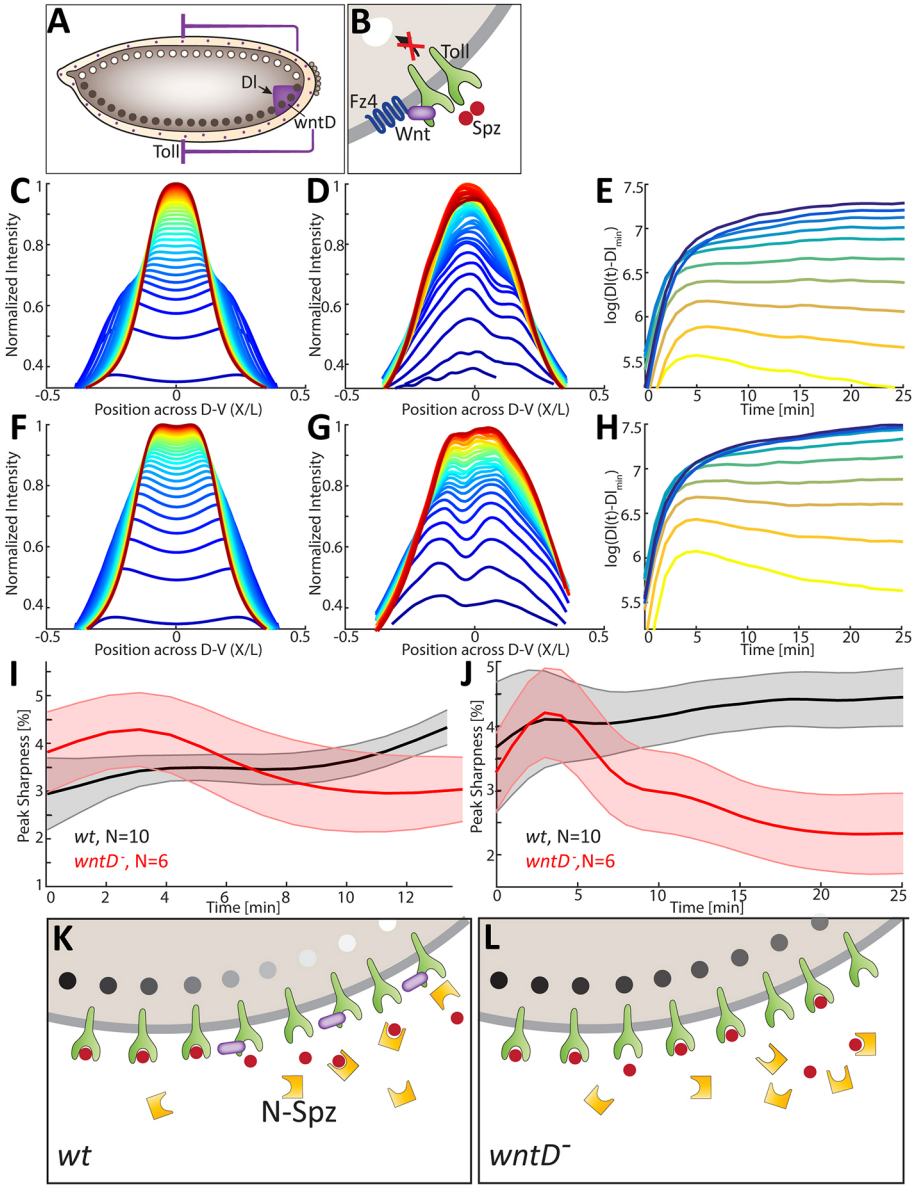

Fig. 4. Shuttling dynamics are impaired in the absence of WntD. (A) A scheme showing the integral feedback loop between Dorsal and WntD. *wntD* expression is restricted to the posterior side of the embryo (purple) and is induced by Dorsal. (B) A scheme showing WntD binding to Fz4, and blocking the binding of Spz to the Toll receptor. (C,F) Simulations of Dl temporal dynamics in the full model for a wild-type (C) and *wntD* mutant (F) embryo (see supplementary Materials and Methods). Time points are color coded as in previous figures. For the *wntD* mutant, the double peak is more prominent and does not fully converge resulting in a flat peak. (D,G) Measured Dorsal temporal dynamics for a wild-type (D) and *wntD* mutant (G) embryo (see Materials and Methods). Time points are color coded as in previous figures, and are 1 min apart. As predicted by the model, the *wntD* mutant exhibits less-efficient shuttling leading to a more prominent double peak, which does not fully converge, resulting in a flat peak. (E,H) Log of Dorsal-GFP intensity temporal dynamics at selected locations along the D-V axis for a wild-type (E) and *wntD* mutant (H) embryo from panels D,G. Locations are color coded as in Fig. 2. Measured values were background subtracted and smoothed in time (see Materials and Methods). The flat peak of the *wntD* mutant embryo results in very similar nuclear Dorsal values over time for the four ventral-most curves, whereas in the wild-type embryo each curve attains a different final value and has different dynamics. (I,J) Peak sharpness over time (calculated as standard deviation/mean in percentage of values close to the peak; see Materials and Methods) in a population of wild-type (wt) embryos (black) and *wntD* mutant embryos (red) during NC 13 (I) and NC 14 (J). Bold lines indicate population mean and surrounding color indicates s.e.m. Number of embryos in each population is indicated. Sharpness in the *wt* population increases over time to a value significantly higher than the *wntD* mutant population. The *wntD* mutant population exhibits an initial increase in peak sharpness due to the prominent double peak, followed by a decrease due to peak flattening. (K) Scheme showing the global attenuation effect of WntD on Toll availability, leading to redirection of active ligand binding towards more ventral positions. (L) In *wntD* mutants, additional Toll receptors become available, leading to increased ligand binding in lateral regions, generating a flatter peak of signaling.

in approximately ten cells, in *wntD* mutants a broader front of up to 15 cells invaginated at the same time (Fig. 5). Thus, the shape of the Dorsal activation gradient is essential for normal patterning and gastrulation. When the final gradient peak is not sharp, a larger cohort of ventral cells takes part in furrow formation.

Timing of *wntD* transcription

wntD mutants display perturbed Dl dynamics already at NC 13 (Fig. 4H, Fig. S5) suggesting that WntD normally exerts its gradient-modulating effects at this early stage. This implies that zygotic expression of *wntD*, its translation, secretion to the peri-vitelline fluid

Development (2019) 146, dev181487. doi:10.1242/dev.181487

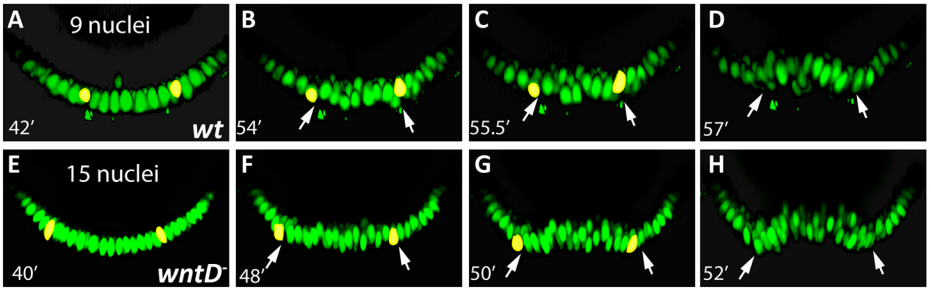

Fig. 5. An enlarged ventral furrow is formed in the absence of WntD. (A-H) Snapshots of cross-sections of a wild-type (*wt*; A-D) and a *wntD* mutant (E-H) embryo expressing Dl-GFP, showing the ventral nuclei during NC 14. Time in NC 14 (in minutes) is indicated. When the first sign of invagination appeared, the most lateral nuclei still displaying positional change were marked (yellow). Working backwards in the movies allowed an accurate count of the nuclei between them prior to invagination.

and diffusion of the protein, have commenced by then. To verify that this is possible, we applied our LSFM visualization setup as a sensitive assay for defining the onset and temporal dynamics of *wntD* expression.

wntD expression is activated by nuclear Dorsal, and is restricted to the posterior region, where Torso signaling relieves Capicua (Cic) repression of *wntD* (Helman et al., 2012). We generated a *wntD*::MS2 reporter, utilizing *wntD* genomic upstream regulatory sequences (Fig. 6A). The early expression profile of this reporter at the posterior part of the embryo mimics the known pattern of *wntD* expression (Rahimi et al., 2016). Importantly, all eight embryos examined expressed *wntD*, implying that excess of Toll signaling, which triggers expression of the WntD 'buffer', is a common consequence of D-V gradient signaling. When monitoring the dynamics of *wntD* expression, the number of nuclei transcribing *wntD* decreased continuously between NCs 12 and 14 (Fig. 6B-F). These results suggest that the WntD protein already exerts its attenuating effect on Toll signaling at an early time. Notably, the diminishing *wntD* expression in NCs 13-14 is attributed to a reduction in Toll signaling rather than in Torso signaling, as constitutive activation of Toll leads to stable *wntD* expression throughout NC 14, indicating the persistence of Torso signaling at this phase (Rahimi et al., 2016). The marked reduction in active transcription of *wntD* at NCs 13-14 is in contrast to the persistence of *wntD* transcripts (Rahimi et al., 2016), suggesting that the transcripts produced at earlier cycles were not yet fully degraded.

Dorsal nuclear re-entry promotes graded accumulation of zygotic *T48* transcripts

The gradient of Dl nuclear localization defines three major domains of zygotic gene expression along the D-V axis. Within each of these regions, several target genes are uniformly expressed. The mesoderm is defined by highest levels of nuclear Dorsal and uniform expression of the zygotic target genes *twist* (*twi*) and *snail* (*sna*) (Rusch and Levine, 1996). There is, however, an additional requirement of a graded zygotic response within the mesoderm: a gradient of apical myosin II recruitment, peaking at the ventral midline, is essential for the ordered apical cell constriction that drives ventral furrow formation (Heer et al., 2017).

Can graded activation of the Toll pathway define not only the broad zones of zygotic gene expression, but also the graded expression pattern of cardinal target genes? We reasoned that this may be the case because, if zygotic expression of Dorsal-target genes depends not only on the final, steady-state level of nuclear Dorsal, but also on the dynamic profile of its accumulation, the signaling output could be further sharpened. A dynamic phase of Dorsal nuclear entry takes place during the initial 20 min of NC 14 (Figs 1F and 2B), the nuclear cycle associated with a major onset of zygotic gene expression. A consequence of these dynamics is that ventral-most nuclei will reach the threshold for expression of a given zygotic gene earlier than more lateral ones. These ventral nuclei will begin to express the gene earlier, therefore expressing it for a longer period than more lateral nuclei. Transcript accumulation should therefore be ventrally biased, if these transcripts are sufficiently stable.

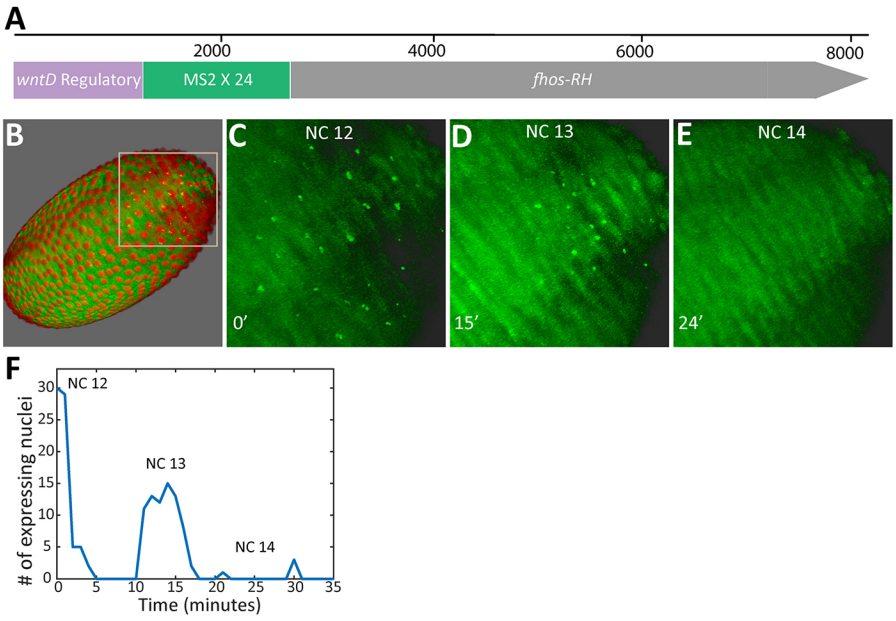

Fig. 6. Dynamics of *wntD* transcription. (A) Schematic of the *wntD*::MS2 reporter. The 1.2 kb regulatory region upstream of the *wntD* coding sequence drives the expression of Fhos-RH with 24 MS2 repeats located at its 5′ end. (B) Light-sheet live imaging of the transcriptional activity of the *wntD* promoter enables quantitative analysis of its dynamics. Embryos express His:RFP, which marks nuclei in red, and the transcriptional activity is indicated by the green signal. (C-F) A constant reduction in the number of nuclei expressing *wntD* is observed from NC 12 onwards, such that by NC 14 no transcription is observed. Because the *wntD* promoter responds to the level of Dorsal, we assume that this reduction reflects the attenuating activity of WntD.

Development (2019) 146, dev181487. doi:10.1242/dev.181487

A zygotic target gene that may lead to graded myosin II distribution is *T48*, because the T48 protein recruits RhoGEF2 to the apical membrane, triggering the accumulation and contractile activity of an apical actomyosin network (Kolsch et al., 2007). We therefore examined whether the dynamics of Dorsal nuclear entry play a role in generating a graded transcriptional response within this region, by monitoring expression of the *T48* target gene. Previous analysis of an MS2 reporter for live *T48* transcription demonstrated that the ventral-most nuclei initiate transcription 15-20 min earlier than the lateral ones (Lim et al., 2017). As *T48* expression requires not only Dorsal but also the product of the Dorsal-target gene *twi* (Urbansky et al., 2016), it will be triggered by Dorsal nuclear entry only at NC 14, and not at earlier cycles.

To examine the consequence of the graded onset of *T48* transcription on mRNA accumulation, we carried out quantitative single-molecule fluorescence *in situ* hybridization (FISH) using *T48* probes. The signal obtained comprised two components: prominent puncta in the nuclei representing active transcription of the gene, and sparse weaker spots in the cytoplasm marking accumulated individual mRNA molecules. We focused on embryos that demonstrated ongoing transcription of *T48* in all ventral nuclei (Fig. 7A), allowing us to monitor the level of active transcription in each nucleus at the time of fixation, as well as the quantity of transcripts that accumulated in the cytoplasm since the onset of transcription. The number of transcribing nuclei in ventral and lateral positions within the expression domain was similar, and the transcription intensity in the different rows appeared comparable (Fig. 7B,C). Most nuclei exhibited two foci, indicating that both chromosomes were transcribing. These features indicate that at the level of individual nuclei, once *T48* transcription is initiated, it progresses at a constant rate independently of the position of the nucleus along the D-V axis.

We next quantified the levels of cytoplasmic *T48* mRNA, using TransQuant software (Bahar Halpern et al., 2015). A clear D-V gradient of cytoplasmic mRNA levels was observed across several cell rows, peaking at the ventral midline (Fig. 7B,D). This result indicates that the *T48* mRNA is sufficiently stable during the temporal window of early NC 14, such that the time of onset of its transcription along the D-V axis, governed by the dynamics of Dorsal nuclear entry, correlates with the level of mRNA that

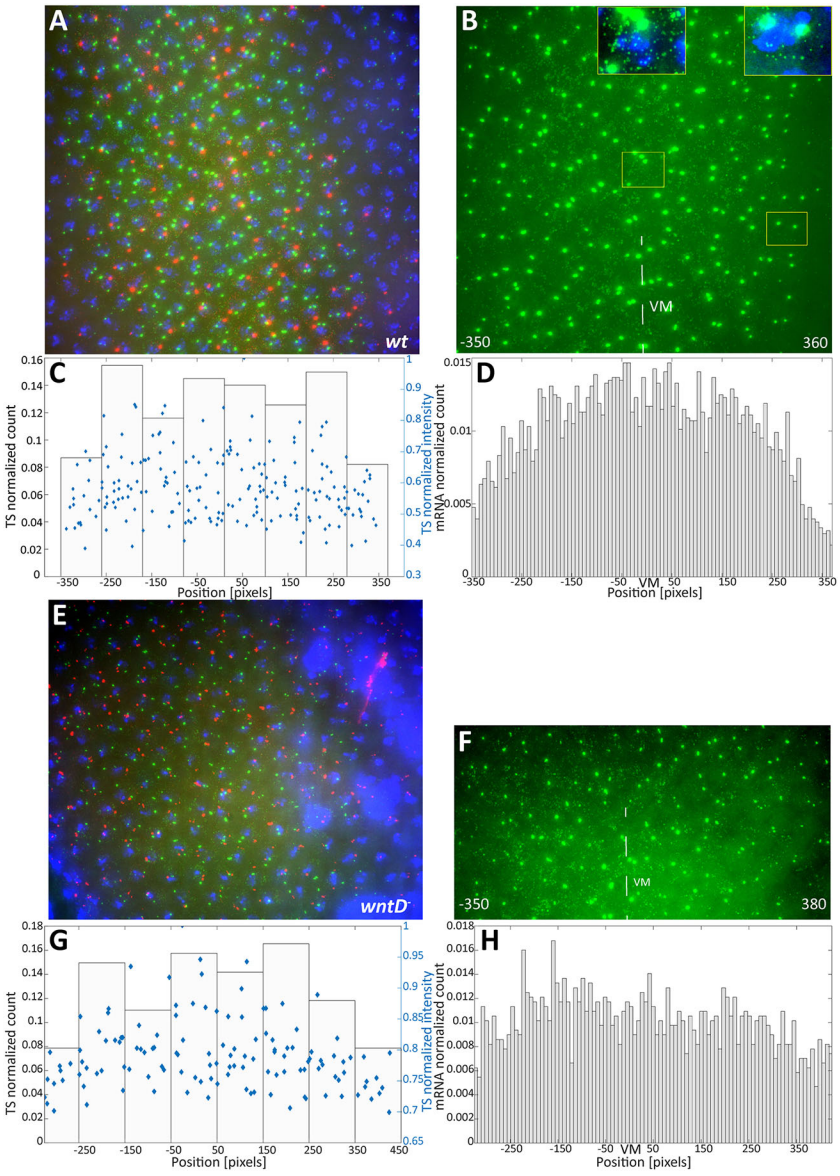

Fig. 7. Graded accumulation of *T48* transcripts. (A) Single-molecule FISH with *T48* (green) and *fog* (red) probes was carried out on wild-type (*wt*) embryos, to mark the ventral domain. We analyzed *T48* signals in embryos that displayed the prominent puncta of transcription sites (TS) in nuclei (DAPI, blue) along the entire ventral domain. (B) Magnified and re-oriented view of a portion of the field shown in A, displaying the *T48* channel alone. The position of the ventral midline (VM) is marked. Weaker cytoplasmic signals (see insets for accentuated views) correspond to individual mature *T48* mRNA molecules. (C) Quantification of the number of TS (displayed as histogram bars) and their intensity (blue dots) at different positions along the D-V axis (0 corresponds to the ventral midline). (D) Quantification of the number of weak cytoplasmic *T48* puncta along the D-V axis. The number of mRNA molecules across the ventral domain displays a gradient that peaks at the ventral midline. We thus conclude that although all nuclei are transcribing *T48* at the same rate, the difference in the onset of transcription coupled with the stability of the mRNA give rise to a graded distribution of mature transcripts. (E,F) A similar analysis was carried out on *wntD* mutant embryos, at the stage when *T48* and *fog* TS are observed across the ventral domain. (G) The number and intensity of *T48* TS along the ventral domain is constant and comparable to wild type. (H) In contrast to wild-type embryos, the accumulation of *T48* transcripts is more uniform, and does not exhibit a graded distribution. We conclude that in the absence of a sharp peak of Dorsal nuclear entry, accumulation of *T48* transcripts is more uniform across the ventral domain.

Development (2019) 146, dev181487. doi:10.1242/dev.181487

accumulates in the adjacent cytoplasm. Dorsal nuclear entry dynamics thus appear to be a crucial factor regulating graded *T48* levels along the D-V axis.

WntD activity facilitates graded accumulation of *T48* transcripts

Because nuclear Dorsal displayed a flat peak in *wntD* mutant embryos, we predicted that these embryos would display an altered distribution of *T48* transcripts. Indeed, single-molecule FISH in *wntD* mutant embryos at the stage when all ventral nuclei express the *T48* gene (Fig. 7E, Fig. S6A-D) revealed a significantly shallower gradient of accumulating *T48* transcripts in the cytoplasm (Fig. 7F-H, Fig. S6E-H). Based on the role of T48 in triggering apical constriction in the invaginating mesoderm (Kolsch et al., 2007), the uniform accumulation of *T48* transcripts could contribute to the broader invaginating front that we observed in *wntD* mutants (Fig. 5). Thus, WntD activity is important not only for restricting the zone of *sna* and *twist* expression, but also for maintaining a sharper peak of Dl nuclear entry, limiting the number of invaginating cells at the onset of gastrulation.

DISCUSSION

Dynamics of the Spz extracellular morphogen gradient

The milieu of the early *Drosophila* embryo poses extreme challenges for the generation and maintenance of extracellular morphogen gradients. Most notably, the peri-vitelline fluid surrounding the embryo facilitates rapid diffusion of molecules (Stein et al., 1991). Analysis of the early morphogen gradients operating in this environment, including ventral Spz/Toll activation and the subsequent BMP gradient patterning the dorsal aspect, should consider this highly dynamic environment. In the case of the Toll pathway, the active Spz ligand is generated by proteolytic processing within the extra-embryonic peri-vitelline fluid in a broad ventral region, defined by the activation domain of the Easter (Ea) protease (Cho et al., 2012). Diffusion-based shuttling can continuously sharpen the Spz activation gradient, within this broad ventral domain. While a variety of experiments and computational analyses indicated the utilization of a 'self-organized shuttling' mechanism that is driven by the Spz pro-domain (Haskel-Ittah et al., 2012), it was imperative to infer the actual dynamics of the process.

We were able to infer the dynamics of the extracellular Spz gradient by following the kinetics of Dorsal-GFP nuclear accumulation in individual live embryos, during the final syncytial nuclear division cycles and the early phase of NC 14. We identified clear hallmarks of ligand shuttling, most notably the initial non-monotonic dynamics (overshoot) predicted in lateral regions, and the presence of two lateral peaks which converge to a central ventral peak. This convergence takes place within a time frame of minutes, and repeats at every nuclear cycle. Because new protein molecules of the extracellular components are continually translated, the ongoing activity of the shuttling process is vital. Therefore, shuttling is important not only for generating the gradient, but also for maintaining it, in the face of rapid diffusion and mixing within the peri-vitelline fluid. Importantly, by ∼10-15 min into NC 14, when the robust induction of transcription of the cardinal zygotic Dorsal-target genes *twi* and *sna* initiates, the nuclear gradient of Dorsal is sharp and a single ventral peak is resolved.

The role of WntD in shaping and buffering the Spz gradient

Having described the dynamics of Dorsal nuclear entry and gradient formation, we were in a position to use our experimental approach in order to examine regulatory processes affecting Toll signaling. The Wnt family ligand WntD provides an essential buffering system to variations in Toll signaling between embryos (Rahimi et al., 2016). WntD is likely to exert its inhibitory effect by associating with the extracellular domain of Toll (Rahimi et al., 2016), thereby reducing the number of Toll receptors that are available for binding Spz. As shuttling relies on competition between ligand binding to the shuttling molecule versus the receptor, this mode of inhibition implies that the effect of WntD would sharpen the shape of the global gradient. The observed dynamics of Dorsal-GFP in *wntD* mutant embryos reported here indeed confirm this prediction. Because WntD impinges on the extracellular properties of the Toll receptor, the active ligand is deposited in more ventral regions, where the concentration of the pro-domain is lower. Thus, WntD does not simply reduce the overall profile of Toll activation, but actually re-directs the ligand from the lateral regions to the ventral domain, as shown by our simulations. We have previously shown that shuttling-dependent accumulation of excess ligand at the center of the field is an effective mechanism to buffer noise. Because activation in this region is already maximal, the excess ligand will not alter the resulting cell fates (Barkai and Shilo, 2009; Shilo and Barkai, 2017).

WntD is produced locally, and the rapid secretion and diffusion of the protein in the peri-vitelline space generates a uniform attenuation of Toll signaling throughout the embryo surface. The rapid timing of processes in the early embryo and the short duration of interphases between nuclear divisions raise the question of whether it is actually possible to produce sufficient levels of WntD that will drive the morphogen distribution to its desired steady-state profile. When monitoring *wntD* transcription directly utilizing the MS2 system, we saw that most, if not all, embryos express *wntD*, indicating that Toll signaling overshoots in most embryos. Furthermore, within single embryos the number of nuclei expressing *wntD* was reduced between NCs 12 and 13, and completely terminated by NC 14, implying that WntD impinges on the Toll gradient and its own expression by this time. The intron-less arrangement of the *wntD* gene and the rapid secretion of the protein, which does not require post-translational modifications (Herr et al., 2012), may facilitate the process.

Dorsal nuclear re-entry refines signaling output

The ventral cohort of zygotic target genes, including *twi* and *sna*, is induced by the Toll activation gradient, and the threshold for their induction corresponds to ∼50% of maximal Dorsal nuclear localization (Kanodia et al., 2009; Liberman et al., 2009). Within the ventral domain, nuclei exhibit a similar level of *sna* transcription (Bothma et al., 2015; Lagha et al., 2013). Robust transcription of these genes ensues at NC 14, after the Dorsal gradient is stabilized and a distinct activation peak generated.

Are there zygotic target genes that respond to the dynamics of Dorsal nuclear targeting, before it stabilizes, within the first 15 min of NC 14? This appears to be the case for *T48*, which encodes a transmembrane protein that facilitates recruitment of RhoGEF2, and ultimately Rho1 and actomyosin, to mediate apical constriction of invaginating mesodermal cells (Kolsch et al., 2007). Graded distribution of myosin II was shown to be crucial for proper invagination of these cells to form the ventral furrow (Heer et al., 2017).

We provide evidence that the graded distribution of *T48* mRNA results from the dynamics of Dorsal nuclear re-entry at NC 14. The ventral-most cells reach the threshold of *T48* induction earlier than

Development (2019) 146, dev181487. doi:10.1242/dev.181487

more lateral cells, and hence will express the gene longer (Lim et al., 2017). Integration of the length of expression along the D-V axis could then lead to a gradient of cytoplasmic *T48* mRNA levels, if the *T48* transcripts are sufficiently stable. This example represents a unique case, in which graded morphogen activation instructs the generation of a gradient of target gene expression. The strict dependence on the timing of transcription initiation provides a mechanism to generate differences in transcript levels between adjacent nuclei along the D-V axis. This mechanism is distinct from a more trivial scenario, in which at steady-state the activity of the morphogen signaling pathway within each nucleus will be linearly translated to the rate of target gene expression.

In conclusion, this work has utilized live imaging of the outcome of Toll pathway activation, to identify and characterize the hallmarks of ligand shuttling (Fig. 8). We find that this process is rapid and takes place continuously throughout the final nuclear division cycles, to generate and maintain a sharp activation gradient in the diffusible environment of the peri-vitelline fluid. WntD impinges on Spz shuttling, and is responsible not only for buffering variability between embryos, but also for generating a sharp activation peak. This peak may be utilized to induce a graded expression of zygotic target genes that are essential for executing processes that drive gastrulation. Thus, diffusion-based ligand shuttling, coupled with a dynamic readout, establishes a refined pattern within the dynamic environment of early embryos.

MATERIALS AND METHODS

Fly stocks and genetics

For the Dorsal-GFP experiments we used Sco/CyO; *dl-GFP*/TM3, Sb flies as the wild-type genotype (DeLotto et al., 2007). The *wntD* null allele $wntD^{CR1}$ served as the *wntD* mutant background. It was generated by CRISPR-induced excision of the entire *wntD* gene, using the following oligonucleotide pairs to generate the guide RNAs: CTTCGAAACCACCTGTAGCTAAAAC, AAACGTTTTAGCTACAGGTGGTTTC; and CTTCGAAGTCCTGTCTGCGTAGCAC, AAACGTGCTACGCAGACAGGACTTC.

$cact^{GL00627}$ (Bloomington *Drosophila* Stock Center stock 37484) was used for *cact* RNAi-based knockdown, and induced maternally by *nos-Gal4*.

To generate *wntD*::*MS2-Fhos-RH*, the 1162 bp region upstream of the *wntD* transcription start site was synthesized and followed by 24 repeats of the MS2 sequence, and placed within the 5′UTR. The sequence was inserted into a pAttB vector with NotI and KpnI sites. The *Fhos-RH* sequence was further ligated into the NotI site to generate *wntD*::MS2-Fhos-RH. Virgin females expressing both MCP::GFP and His:RFP were crossed with males of the reporter line *wntD*::*MS2-Fhos-RH* to collect embryos for imaging.

Live imaging

Embryos were imaged using a Light Sheet Z.1 microscope (Zeiss) equipped with two sCMOS cameras PCO-Edge, 10× excitation objectives and Light Sheet Z.1 detection optics 20×/1.0 (water immersion). The embryos were collected, dechorionated, and up to four embryos were sequentially mounted perpendicularly into a glass capillary (Brand) in a 1% low melting agarose solution (Roth). Imaging was performed using dual-side illumination, zoom ×0.8. GFP excitation: 488 nm, emission/detection - BP 505-545; RFP excitation: 561 nm, emission/detection: BP 575-615 nm.

sm-FISH

Stellaris RNA FISH probe sets for the *T48* gene (5′ UTR and coding, not including the 3′ UTR), were designed by Stellaris Probe Designer and purchased from LGC Biosearch Technologies. Three hours after egg laying (AEL) *wt* embryos were fixed for 25 min in 4% formaldehyde, washed in methanol and kept at −20°C. The following day, embryos were washed in methanol and then in ethanol, rocked in 90% xylene, 10% ethanol for 1 h, post-fixed in 4% paraformaldehyde/PBS/0.05 M EGTA for 25 min, washed three times (10 min each wash), then incubated for 6 min with Proteinase K and post-fixed again. Embryos were transferred gradually to 10% FA (Formamide Deionized, Thermo Fisher Scientific, AM9342) in 2× SSC+10 µg/ml ssDNA preheated to 37°C and prehybridized for 30 min at 37°C. Hybridization buffer included 10% FA, 10% dextran, 2 mg/ml bovine serum albumin (Thermo Fisher, AM2616), RVC (Ribonucleoside Vanadyl Complex, NEB, S1402) and ssDNA+ tRNA in 2× SSC, containing the probe set (1 ng/µl) (Trcek et al., 2017). Hybridization was carried out overnight at 37°C. Next morning the embryos were shaken gently and incubated for another 30 min. Embryos were washed twice for 30 min each wash at 37°C with 10% FA in 2× SSC+10 µg/ml ssDNA and gradually transferred to PBS-0.5% Tween and mounted with Vectashield+DAPI Mounting Medium (Vector Laboratories). Fluorescence was visualized with a Nikon Eclipse Ti2 microscope, and analyzed by the TransQuant script as previously published (Bahar Halpern and Itzkovitz, 2016). TS intensities were measured using ImageJ.

LSFM movie analysis

Projection to 2D

To enable quantitative analysis of the nuclear Dl gradient, we projected the 3D scans of the embryo from the light-sheet microscope, into a 2D flat surface, for every time point imaged. This was possible, because all the nuclei are arranged on the surface of the embryo, the shape of which resembles an ellipsoid. This ellipsoid can be projected onto a 2D surface, which contains all the nuclei and therefore the entire nuclear Dorsal gradient. To this end, we used an area-preserving transformation with minimal distortion far from the anterior and posterior poles, implemented by the IMSANE tissue cartography tool (Heemskerk and Streichan, 2015). IMSANE was used with the following specifications: Planar Illastik surface detector and cylinder chart type. Surface detection was performed at the last

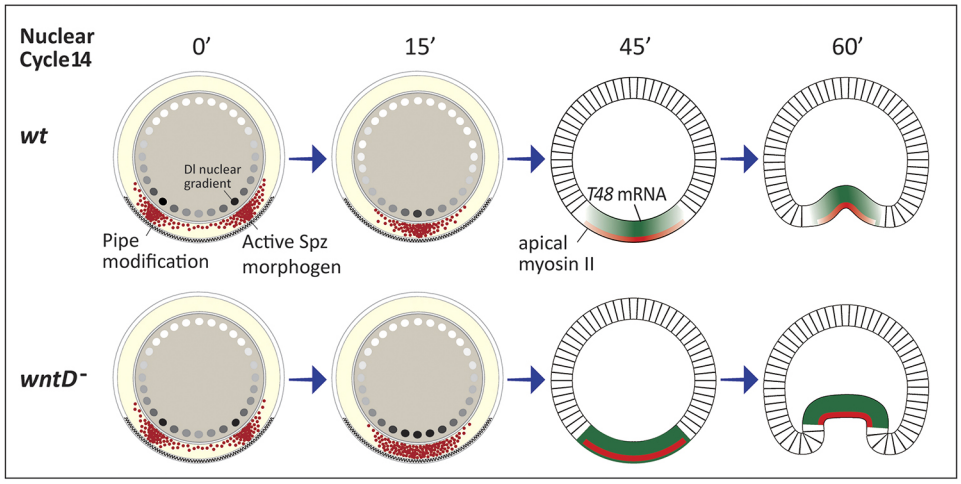

Fig. 8. Dynamics of Spz shuttling establishes pattern. The shuttling mechanism operates within a wide D-V domain predefined by Pipe expression during oogenesis. Initially, a double-peak distribution of the Spz morphogen in the peri-vitelline space is observed. In wild-type (*wt*) embryos, shuttling operates efficiently to concentrate the Spz morphogen to a single sharp peak. The dynamics of the Dorsal gradient are utilized by the embryo to induce graded accumulation of zygotic transcripts, which facilitate recruitment of RhoGEF2 and ultimately Rho1 and actomyosin, to drive apical constriction of invaginating future mesodermal cells. Loss of WntD ($wntD^{-}$) renders shuttling less efficient, leading to a flattened peak of morphogen distribution resulting in a broader gastrulation furrow.

time point for each embryo, and the detected surface was then used to project all earlier time points. Because the embryo is, to a good approximation, a cylinder apart from the anterior and posterior poles, embryo circumference was defined as the largest circumference of the ellipsoid fitted to the embryo surface by IMSANE.

Nuclei segmentation

The nuclei were detected separately for each time point, using the following segmentation method. Automated local thresholding of the image was carried out in order to create a binary mask. This was done in ImageJ using the Bernsen algorithm with a contrast threshold of 15. The resulting binary mask underwent further refinement to segment the nuclei using MATLAB image analysis filters as follows: (1) all connected objects in the mask large enough to be nuclei (over 50 pixels in size) were located and classified into three size groups (small, 50-150 pixels; medium, 150-600 pixels; large, 600 pixels and over), (2) each size group underwent erosion using 'imerode' and then dilation using 'imdilate' with appropriate filter sizes for each group, and (3) objects belonging to the 'large' group underwent another round of erosion and dilation with same filter size as in the first round.

The resulting objects in the binary mask were filtered by size to exclude objects too small (under 50 pixels) or too large (over 3000 pixels) to be a single nucleus. Nuclei locations were detected by overlaying the mask on the original image.

Measuring the nuclear Dorsal gradient around the A-P midline

Gradient measurement was performed by first manually discarding all time points between the nuclear cycles. Then, for every detected nucleus, for all remaining time points, the value of nuclear Dorsal was calculated as the mean intensity inside the nucleus (located by the above segmentation method). The location of the A-P midline was manually selected for each embryo. A rectangular area around the A-P midline was then defined. The width of the area along the A-P axis was 15% of the entire A-P length and it spanned the entire D-V axis. For NC 14, this definition corresponds to approximately eight to ten columns of nuclei closest to the A-P midline. Only the nuclei inside this area were taken into account for gradient measurement; monitoring several columns of nuclei along the A-P axis gave rise to averaging of Dorsal nuclear intensity along this small window. The spatial axis for the gradient was defined as a relative axis, x/L, indicating the location on the D-V axis, x, divided by embryo circumference, L. In order to assign a location on this relative D-V axis for each nucleus, the location of the D-V midline was manually selected and defined as $x/L=0$. This resulted in the raw intensity function, $Dl_{raw}(x/L, t)$ measuring nuclei intensity along the relative D-V axis, over time. This function, $Dl_{raw}(x/L, t)$, was then smoothened in space for each time point separately using the MATLAB 'smooth' function with a smoothing coefficient of 0.23. The smoothened data was then fitted by a smoothing spline using the MATLAB 'fit' function and evaluated on 1000 linearly spaced x/L locations. The resulting function, $Dl_{smooth}(x/L, t)$, was plotted in the main text figures.

Dorsal gradient as a function of time, at specific locations along the D-V axis

For the calculation of Dorsal nuclear intensity over time at a specific location, $\tilde{x}/L$, we used $Dl_{smooth}(x/L, t)$ at that location: $Dl_{smooth}(\tilde{x}/L, t)$. Background subtracted values were calculated separately for each nuclear cycle by subtracting the minimal intensity observed in a nucleus for that nuclear cycle. $Dl_{smooth}(\tilde{x}/L, t)$ was then smoothened in time using the MATLAB 'smooth' function with the LOESS method and a smoothing coefficient of 0.5. It was then fitted with a smoothing spline, resulting in the function $Dl^{fitted}_{\tilde{x}/L}(t)$. The temporal derivative of nuclear Dorsal, at a specific location, $\tilde{x}/L$, was calculated by applying a third-order finite differences formula to $Dl^{fitted}_{\tilde{x}/L}(t)$ and then smoothing using 'smooth' with a smoothing coefficient of 0.6 and fitting a smoothing spline.

Measuring peak sharpness

The peak sharpness measure for an embryo was calculated based on the values of $Dl_{smooth}(x/L, t)$, around the ventral-most location. For each time point, $\tilde{t}$, $Dl_{smooth}(x/L, \tilde{t})$ was normalized by dividing by its maximal value at $\tilde{t}$. Peak sharpness was then calculated as the standard deviation divided by the mean, in percentage, of values close to the peak, i.e. within the range $(x/L)\in[-0.1, 0.1]$. This measure captures how different from each other are values close to the peak.

Acknowledgements

We are grateful to Y. Addadi and O. Golani for help in acquisition and analysis of LSFM images, to S. Itzkovitz for advice on single-molecule FISH, and S. Streichan for support in 3D image processing. Imaging using the light-sheet microscope was made possible thanks to the de Picciotto-Lesser Cell Observatory in memory of Wolf and Ruth Lesser. We thank the members of the Shilo and Barkai labs for fruitful discussions.

Competing interests

The authors declare no competing or financial interests.

Author contributions

Conceptualization: N.R., I.A., E.D.S., N.B., B.-Z.S.; Methodology: N.R., I.A., S.C.; Software: I.A.; Formal analysis: N.R., I.A.; Investigation: N.R., I.A., S.C., B.-Z.S.; Resources: I.A., S.C.; Data curation: N.R., I.A.; Writing - original draft: I.A., N.B., B.-Z.S.; Writing - review & editing: I.A., E.D.S., N.B., B.-Z.S.; Visualization: I.A.; Supervision: E.D.S., N.B., B.-Z.S.; Funding acquisition: E.D.S., N.B., B.-Z.S.

Funding

This work was supported by a European Research Council advanced grant (338660 to N.B.) and a US-Israel Binational grant (2015063 to E.D.S. and B.-Z.S.). N.B. is the incumbent of the Lorna Greenberg Scherzer Professorial chair, and B.-Z.S. is the incumbent of the Hilda and Cecil Lewis Professorial chair in Molecular Genetics.

Supplementary information

Supplementary information available online at
http://dev.biologists.org/lookup/doi/10.1242/dev.181487.supplemental

References

Bahar Halpern, K. and Itzkovitz, S. (2016). Single molecule approaches for quantifying transcription and degradation rates in intact mammalian tissues. *Methods* **98**, 134-142. doi:10.1016/j.ymeth.2015.11.015

Bahar Halpern, K., Caspi, I., Lemze, D., Levy, M., Landen, S., Elinav, E., Ulitsky, I. and Itzkovitz, S. (2015). Nuclear retention of mRNA in mammalian tissues. *Cell Rep.* **13**, 2653-2662. doi:10.1016/j.celrep.2015.11.036

Barkai, N. and Shilo, B.-Z. (2009). Robust generation and decoding of morphogen gradients. *Cold Spring Harb. Perspect. Biol.* **1**, a001990. doi:10.1101/cshperspect.a001990

Belvin, M. P. and Anderson, K. V. (1996). A conserved signaling pathway: the Drosophila toll-dorsal pathway. *Annu. Rev. Cell Dev. Biol.* **12**, 393-416. doi:10.1146/annurev.cellbio.12.1.393

Ben-Zvi, D., Shilo, B.-Z., Fainsod, A. and Barkai, N. (2008). Scaling of the BMP activation gradient in Xenopus embryos. *Nature* **453**, 1205-1211. doi:10.1038/nature07059

Ben-Zvi, D., Fainsod, A., Shilo, B.-Z. and Barkai, N. (2014). Scaling of dorsal-ventral patterning in the Xenopus laevis embryo. *BioEssays* **36**, 151-156. doi:10.1002/bies.201300136

Bothma, J. P., Garcia, H. G., Ng, S., Perry, M. W., Gregor, T. and Levine, M. (2015). Enhancer additivity and non-additivity are determined by enhancer strength in the Drosophila embryo. *eLife* **4**, e07956. doi:10.7554/eLife.07956

Carrell, S. N., O'Connell, M. D., Jacobsen, T., Pomeroy, A. E., Hayes, S. M. and Reeves, G. T. (2017). A facilitated diffusion mechanism establishes the Drosophila Dorsal gradient. *Development* **144**, 4450-4461. doi:10.1242/dev.155549

Cho, Y. S., Stevens, L. M., Sieverman, K. J., Nguyen, J. and Stein, D. (2012). A ventrally localized protease in the Drosophila egg controls embryo dorsoventral polarity. *Curr. Biol.* **22**, 1013-1018. doi:10.1016/j.cub.2012.03.065

DeLotto, Y. and DeLotto, R. (1998). Proteolytic processing of the Drosophila Spätzle protein by easter generates a dimeric NGF-like molecule with ventralising activity. *Mech. Dev.* **72**, 141-148. doi:10.1016/S0925-4773(98)00024-0

DeLotto, R., DeLotto, Y., Steward, R. and Lippincott-Schwartz, J. (2007). Nucleocytoplasmic shuttling mediates the dynamic maintenance of nuclear Dorsal levels during Drosophila embryogenesis. *Development* **134**, 4233-4241. doi:10.1242/dev.010934

di Pietro, F. and Bellaïche, Y. (2018). Actin network discussion during mitotic pseudo-furrowing. *Dev. Cell* **45**, 539-541. doi:10.1016/j.devcel.2018.05.018

Dorfman, R. and Shilo, B. Z. (2001). Biphasic activation of the BMP pathway patterns the Drosophila embryonic dorsal region. *Development* **128**, 965-972.

Eldar, A., Dorfman, R., Weiss, D., Ashe, H., Shilo, B.-Z. and Barkai, N. (2002). Robustness of the BMP morphogen gradient in Drosophila embryonic patterning. *Nature* **419**, 304-308. doi:10.1038/nature01061

Foe, V. E. and Alberts, B. M. (1983). Studies of nuclear and cytoplasmic behaviour during the five mitotic cycles that precede gastrulation in Drosophila embryogenesis. *J. Cell Sci.* **61**, 31-70.
Gabay, L., Seger, R. and Shilo, B. Z. (1997). MAP kinase in situ activation atlas during Drosophila embryogenesis. *Development* **124**, 3535-3541.
Genikhovich, G., Fried, P., Prünster, M. M., Schinko, J. B., Gilles, A. F., Fredman, D., Meier, K., Iber, D. and Technau, U. (2015). Axis patterning by BMPs: Cnidarian network reveals evolutionary constraints. *Cell Rep.* **10**, 1646-1654. doi:10.1016/j.celrep.2015.02.035
Green, J. B. A. and Sharpe, J. (2015). Positional information and reaction-diffusion: two big ideas in developmental biology combine. *Development* **142**, 1203-1211. doi:10.1242/dev.114991
Haskel-Ittah, M., Ben-Zvi, D., Branski-Arieli, M., Schejter, E. D., Shilo, B.-Z. and Barkai, N. (2012). Self-organized shuttling: generating sharp dorsoventral polarity in the early Drosophila embryo. *Cell* **150**, 1016-1028. doi:10.1016/j.cell.2012.06.044
Heemskerk, I. and Streichan, S. J. (2015). Tissue cartography: compressing bio-image data by dimensional reduction. *Nat. Methods* **12**, 1139-1142. doi:10.1038/nmeth.3648
Heer, N. C., Miller, P. W., Chanet, S., Stoop, N., Dunkel, J. and Martin, A. C. (2017). Actomyosin-based tissue folding requires a multicellular myosin gradient. *Development* **144**, 1876-1886. doi:10.1242/dev.146761
Helman, A., Lim, B., Andreu, M. J., Kim, Y., Shestkin, T., Lu, H., Jimenez, G., Shvartsman, S. Y. and Paroush, Z. (2012). RTK signaling modulates the Dorsal gradient. *Development* **139**, 3032-3039. doi:10.1242/dev.075812
Herr, P., Hausmann, G. and Basler, K. (2012). WNT secretion and signalling in human disease. *Trends Mol. Med.* **18**, 483-493. doi:10.1016/j.molmed.2012.06.008
Kanodia, J. S., Rikhy, R., Kim, Y., Lund, V. K., DeLotto, R., Lippincott-Schwartz, J. and Shvartsman, S. Y. (2009). Dynamics of the Dorsal morphogen gradient. *Proc. Natl. Acad. Sci. USA* **106**, 21707-21712. doi:10.1073/pnas.0912395106
Kolsch, V., Seher, T., Fernandez-Ballester, G. J., Serrano, L. and Leptin, M. (2007). Control of Drosophila gastrulation by apical localization of adherens junctions and RhoGEF2. *Science* **315**, 384-386. doi:10.1126/science.1134833
Lagha, M., Bothma, J. P., Esposito, E., Ng, S., Stefanik, L., Tsui, C., Johnston, J., Chen, K., Gilmour, D. S., Zeitlinger, J. et al. (2013). Paused Pol II coordinates tissue morphogenesis in the Drosophila embryo. *Cell* **153**, 976-987. doi:10.1016/j.cell.2013.04.045
Lapraz, F., Besnardeau, L. and Lepage, T. (2009). Patterning of the dorsal-ventral axis in echinoderms: insights into the evolution of the BMP-chordin signaling network. *PLoS Biol.* **7**, e1000248. doi:10.1371/journal.pbio.1000248
Lecuit, T., Brook, W. J., Ng, M., Calleja, M., Sun, H. and Cohen, S. M. (1996). Two distinct mechanisms for long-range patterning by Decapentaplegic in the Drosophila wing. *Nature* **381**, 387-393. doi:10.1038/381387a0
Liberman, L. M., Reeves, G. T. and Stathopoulos, A. (2009). Quantitative imaging of the Dorsal nuclear gradient reveals limitations to threshold-dependent patterning in Drosophila. *Proc. Natl. Acad. Sci. USA* **106**, 22317-22322. doi:10.1073/pnas.0906227106
Lim, B., Levine, M. and Yamazaki, Y. (2017). Transcriptional Pre-patterning of Drosophila Gastrulation. *Curr. Biol.* **27**, 610. doi:10.1016/j.cub.2017.01.067
Lynch, J. A. and Roth, S. (2011). The evolution of dorsal-ventral patterning mechanisms in insects. *Genes Dev.* **25**, 107-118. doi:10.1101/gad.2010711
Morisato, D. and Anderson, K. V. (1994). The spätzle gene encodes a component of the extracellular signaling pathway establishing the dorsal-ventral pattern of the Drosophila embryo. *Cell* **76**, 677-688. doi:10.1016/0092-8674(94)90507-X
Nellen, D., Burke, R., Struhl, G. and Basler, K. (1996). Direct and long-range action of a DPP morphogen gradient. *Cell* **85**, 357-368. doi:10.1016/S0092-8674(00)81114-9
Rahimi, N., Averbukh, I., Haskel-Ittah, M., Degani, N., Schejter, E. D., Barkai, N. and Shilo, B.-Z. (2016). A WntD-dependent integral feedback loop attenuates variability in Drosophila toll signaling. *Dev. Cell* **36**, 401-414. doi:10.1016/j.devcel.2016.01.023
Reversade, B. and De Robertis, E. M. (2005). Regulation of ADMP and BMP2/4/7 at opposite embryonic poles generates a self-regulating morphogenetic field. *Cell* **123**, 1147-1160. doi:10.1016/j.cell.2005.08.047
Rusch, J. and Levine, M. (1996). Threshold responses to the dorsal regulatory gradient and the subdivision of primary tissue territories in the Drosophila embryo. *Curr. Opin. Genet. Dev.* **6**, 416-423. doi:10.1016/S0959-437X(96)80062-1
Schejter, E. D. and Wieschaus, E. (1993). Functional elements of the cytoskeleton in the early Drosophila embryo. *Annu. Rev. Cell Biol.* **9**, 67-99. doi:10.1146/annurev.cb.09.110193.000435
Schneider, D. S., Jin, Y., Morisato, D. and Anderson, K. V. (1994). A processed form of the Spatzle protein defines dorsal-ventral polarity in the Drosophila embryo. *Development* **120**, 1243-1250.
Shilo, B.-Z. and Barkai, N. (2017). Buffering global variability of morphogen gradients. *Dev. Cell* **40**, 429-438. doi:10.1016/j.devcel.2016.12.012
Shilo, B.-Z., Haskel-Ittah, M., Ben-Zvi, D., Schejter, E. D. and Barkai, N. (2013). Creating gradients by morphogen shuttling. *Trends Genet.* **29**, 339-347. doi:10.1016/j.tig.2013.01.001
Shimmi, O., Umulis, D., Othmer, H. and O'Connor, M. B. (2005). Facilitated transport of a Dpp/Scw heterodimer by Sog/Tsg leads to robust patterning of the Drosophila blastoderm embryo. *Cell* **120**, 873-886. doi:10.1016/j.cell.2005.02.009
Stein, D., Roth, S., Vogelsang, E. and Nüsslein-Volhard, C. (1991). The polarity of the dorsoventral axis in the Drosophila embryo is defined by an extracellular signal. *Cell* **65**, 725-735. doi:10.1016/0092-8674(91)90381-8
Tanimoto, H., Itoh, S., ten Dijke, P. and Tabata, T. (2000). Hedgehog creates a gradient of DPP activity in Drosophila wing imaginal discs. *Mol. Cell* **5**, 59-71. doi:10.1016/S1097-2765(00)80403-7
Trcek, T., Lionnet, T., Shroff, H. and Lehmann, R. (2017). mRNA quantification using single-molecule FISH in Drosophila embryos. *Nat. Protoc.* **12**, 1326-1348. doi:10.1038/nprot.2017.030
Urbansky, S., Gonzalez Avalos, P., Wosch, M. and Lemke, S. (2016). Folded gastrulation and T48 drive the evolution of coordinated mesoderm internalization in flies. *eLife* **5**, e18318. doi:10.7554/eLife.18318
van der Zee, M., Stockhammer, O., von Levetzow, C., Nunes da Fonseca, R. and Roth, S. (2006). Sog/Chordin is required for ventral-to-dorsal Dpp/BMP transport and head formation in a short germ insect. *Proc. Natl. Acad. Sci. USA* **103**, 16307-16312. doi:10.1073/pnas.0605154103
Wang, Y.-C. and Ferguson, E. L. (2005). Spatial bistability of Dpp-receptor interactions during Drosophila dorsal-ventral patterning. *Nature* **434**, 229-234. doi:10.1038/nature03318
Weber, A. N. R., Tauszig-Delamasure, S., Hoffmann, J. A., Lelièvre, E., Gascan, H., Ray, K. P., Morse, M. A., Imler, J.-L. and Gay, N. J. (2003). Binding of the Drosophila cytokine Spätzle to Toll is direct and establishes signaling. *Nat. Immunol.* **4**, 794-800. doi:10.1038/ni955
Wolpert, L. (1971). Positional information and pattern formation. *Curr. Top. Dev. Biol.* **6**, 183-224. doi:10.1016/S0070-2153(08)60641-9
Wotton, K. R., Alcaine-Colet, A., Jaeger, J. and Jiménez-Guri, E. (2017). Non-canonical dorsoventral patterning in the moth midge Clogmia albipunctata. *Evodevo* **8**, 20. doi:10.1186/s13227-017-0083-9
Zhang, Y., Yu, J. C., Jiang, T., Fernandez-Gonzalez, R. and Harris, T. J. C. (2018). Collision of expanding actin caps with actomyosin borders for cortical bending and mitotic rounding in a syncytium. *Dev. Cell* **45**, 551-564.e554. doi:10.1016/j.devcel.2018.04.024